IN21B-0487

Geoffrey Ely, gely@ucsd.edu,
Jean-Bernard Minster
Institute of Geophysics and Planetary Physics
Scripps Institution of Oceanography
University of California, San Diego

Steven Day
Department of Geological Sciences
San Deigo State University

The Support Operator Rupture Dynamics (SORD) code provides a highly scalable computational tool for modeling spontaneous rupture on a non-planar fault surface embedded in a heterogeneous medium. In the first section of this poster, we used an assortment of test problems to verify different aspects of SORD. The second section uses SORD to model a M_W7.6 earthquake on the southern San Andreas fault.

References

Campbell, K. W., and Y. Bozorgnia (2007), Campbell-Bozorgnia NGA ground motion relations for the geometric mean horizontal component of peak and spectral ground motion parameters, *Tech. Rep. PEER 2007/02*, Pacific Earthquake Engineering Research Center.

Day, S. M., J. Bielak, D. Dreger, R. Graves, S. Larsen, K. B. Olsen, and A. Pitarka (2001), Tests of 3D elastodynamic codes: Final report for Lifelines Project 1A01, *Tech. rep.*, Pacific Earthquake Engineering Research Center.

Ely, G. P., S. M. Day, and J.-B. Minster (2007), A support-operator method for visco-elastic wave modeling in 3d heterogeneous media, *Geophys. J. Int.*, in press, doi: 10.1111/j.1365-246X.2007.03633.x.

Harris, R. A., and R. J. Archuleta (2004), Earthquake rupture dynamics: Comparing the numerical simulation methods, *Eos Trans. AGU*, *85*(34), 321, doi:10.1029/2004EO340003.

Kawase, H. (1988), Time-domain response of a semi-circular canyon for incident SV, P, and Rayleigh waves calculated by the discrete wavenumber boundary element method, *Bull. Seism. Soc. Am.*, *78*(4), 1415–1437.

Magistrale, H., S. M. Day, R. W. Clayton, and R. W. Graves (2000), The SCEC Southern California reference three-dimensional seismic velocity model version 2, *Bull. Seism. Soc. Am.*, *90*(6B), S65–76, doi:10.1785/0120000510.

Olsen, K. B., S. M. Day, J.-B. Minster, Y. Cui, A. Chourasia, M. Faerman, R. Moore, P. Maechling, and T. Jordan (2006), Strong shaking in Los Angeles expected from southern San Andreas earthquake, *Geophys. Res. Lett.*, *33*(L07305), doi:10.1029/2005GL025472.

Olsen, K. B., S. M. Day, J.-B. Minster, Y. Cui, A. Chourasia, D. Okaya, P. Maechling, and T. Jordan (2007), TeraShake2: Simulation of m_w7.7 earthquakes on the southern San Andreas fault with spontaneous rupture description, *Bull. Seism. Soc. Am., in review.*

Peyrat, S., K. B. Olsen, and R. Madariaga (2001), Dynamic modeling of the 1992 landers earthquake, *J. Geophys. Res.*, *106*(B11), 26,467, doi:10.1029/2001JB000205.

Sánchez-Sesma, F. J., and M. Campillo (1991), Diffraction of P, SV, and rayleigh waves by topographic features: A boundary integral formulation, *Bull. Seism. Soc. Am.*, *81*(6), 2234–2253.

Wong, H. L. (1982), Effect of surface topography on the diffraction of P, SV, and Rayleigh waves, *Bull. Seism. Soc. Am.*, *72*(4), 1167–1183.

Verification of SORD

LOH.2 Test

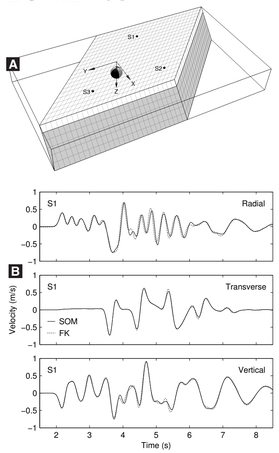

One of the validation problems used by Day, el al (2001) for testing a variety of wave propagation codes, LOH.2 consists of a layer over a half-space (with differing material properties) and a buried double-couple point source. In our testing of SORD, we apply two 45° simple shears to a Cartesian mesh resulting in 55° of total shear. Figure [A] shows a low resolution schematic of the mesh used for the simulation. Anisotropy of wave propagation due to sheared elements is assessed by observing ground motion at different azimuths to the source. A representative case for sensor S1 shows good agreement with a frequency-wavenumber solution [B], when the resolution is greater than 10 points per wavelength.

Canyon Test

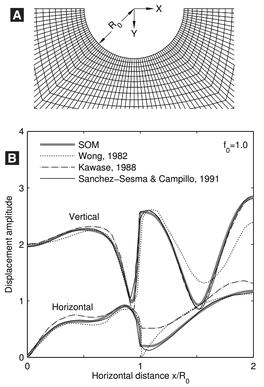

The canyon test aims to verify the free surface boundary condition in the presence of topographic features. A vertically incident P wave on a semi-circular canyon [A] presents a challenging problem, as significant energy is converted to SV and Rayleigh waves, and relative amplification is highly variable in and around the canyon. The problem has been studied using various boundary integral methods, providing independent solutions. Plot [B] shows surface displacement amplitude, at normalized frequency $f_0 = wR_0/2\pi V_S$, as a function of horizontal distance from the center of the canyon. This frequency corresponds to a P wavelength equal to the canyon width, and an S wavelength equal to R_0. Amplitudes are relative to that of the source wavelet. Results agree particularly well with the more recent of the previous studies.

TPV3 Dynamic Rupture Test

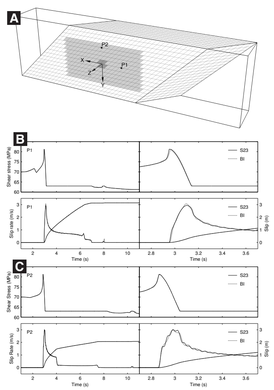

For dynamic rupture verification, we use 'The Problem' version 3 (TPV3) developed for the SCEC Spontaneous Rupture Code-Validation Workshop (Harris and Archuleta, 2004). The problem, consisting of a planar fault within an infinite elastic isotropic medium, can also be solved using the boundary integral (BI) methods. We use a similar shearing of the mesh as the LOH.2 test. The schematic [A] shows the mesh for the far fault block. The near fault block (a mirror image of the far block) is removed to allow viewing of the fault surface. The 30 x 15 km slipping portion of the fault is shaded gray, and the nucleation area is shaded dark gray. Results agree closely with BI. Plot [B] shows the time histories for a point of mode II rupture, and [C] shows a mode III point, with the right hand panel magnified in time to see detail at the rupture arrival time.

Accuracy of Sheared Mesh Solutions

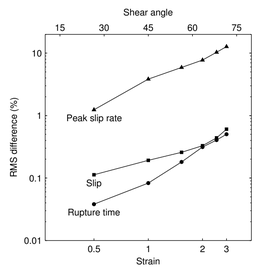

Likely the most useful type of mesh deformation for earthquake rupture problems, is shearing normal to fault, where the fault element remain rectangular, and volume elements are deflected towards or away from the slip vector. This geometry accommodates the case of dip-slip rupture on a dipping fault, as well as the case of a vertical strike-slip fault with variable strike. Modeling low-angle thrust faults, in particular, may require drastic element deformations of this type, so it is important to understand the numerical affects of such deformations. We perform a series of TPV3 tests, while shearing angle was varied, up to a maximum of 73°. The grid-induced errors increase with mesh-shear angle, with the logarithm of error approximately proportional to angle over the range tested. At 73°, RMS misfits are about 10% for peak slip rate, and 0.5% for both rupture time and total slip, indicating that the method--which up to now we have applied mainly to near-vertical strike-slip faulting--also is capable of handling geometries appropriate to low-angle surface-rupturing thrust earthquakes.

Application to the TeraShake Scenario

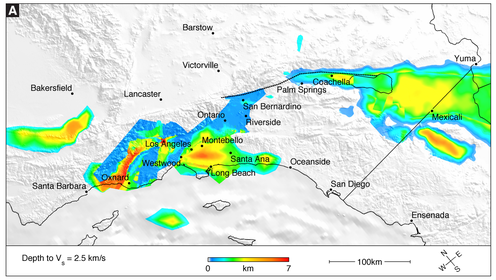

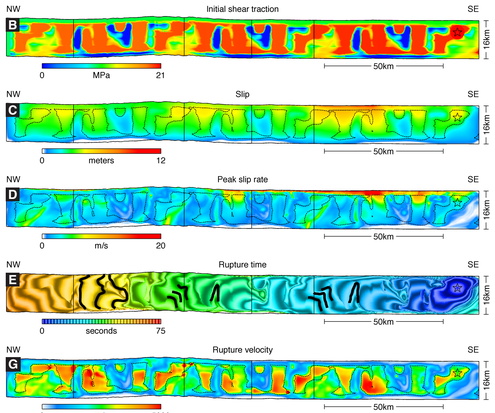

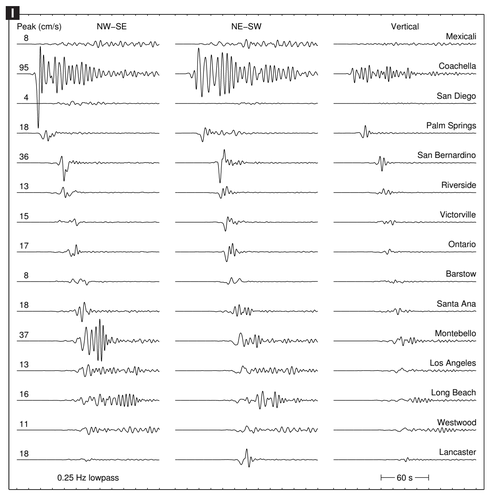

The TeraShake2 simulations, by Olsen et al (2007), simulated spontaneous rupture on 200 kilometers of the southern San Andreas fault, for a M_W7.7 earthquake. We reexamine that scenario using the SORD code in the frequency range of 0 to 0.25 Hz. Differences with TeraShake2 are that we use SCEC Community Velocity Model (SCEC-CVM) version 4.0 and true topography for southern California (TeraShake2 use version 3.0 and a flat free surface).

[A] Map of the simulation region showing the fault location (dashed line) and the sedimentary basin depth from the SCEC-CVM version 4.0 as defined by the depth to 2.5 km/s S-wave velocity horizon.

[B] Heterogeneous initial shear traction on the fault plane is derived from a dynamic inversion of the M7.3 1992 Landers event by Peyrat et al (2001). To scale the Landers event up to the 200 km fault length, the distribution is replicated multiple time laterally.

[C] Highest slip occurs in regions of high initial traction demarcated by dashed lines (asperities).

[D] Highest peak slip rate at depth occurs outside of the asperities, as a result of rupture front focusing. This suggests a mechanism by which high-frequency components of the slip function can be at least partially disjointed from low-frequency components.

[E] Heavy contours of the initial rupture time highlight episodes of rupture front focusing that lead to the high peak slip rates.

[F] A space-time plot of depth averaged slip rate shows the rupture is pulse-like with an overall rupture velocity less than the Rayleigh velocity (V_R).

[G] Local rupture velocity often exceeds the S-wave speed inside asperities.

[H] A histogram of rupture velocity (for the areas excluding the sedimentary basins) shows that the upper bound on the rupture velocity is about $\sqrt{2}V_S$, the velocity at which S-wave radiation vanishes for mode II rupture. A local minimum occurs around V_S, reflecting that mode II rupture propagation in not possible in the range between V_R and V_S.

[I] Ground motion time histories reveal long lasting reverberations at Los Angeles basin sites. As observed in TeraShake, basin guided wave produce exceptionally strong motion at Montebello, though we find smaller amplification than did TeraShake. The smaller amplification may be due to a shallower Chino basin in SCEC-CVM version 4.0 compared to version 3.0, that was used for Terashake.

[J] Empirically determined attenuations relations, derived from earthquake catalogs, give statistical predictions of ground motion based on the type and size of the earthquake, and the properties of the receiver location. They provide one of the few means to compare hypothetical earthquake scenarios to real data. Peak ground velocity (PGV) is compared to the Campbell and Bozorgnia (2007) 'next generation' attenuation relation (CB-NGA). Though agreement is generally within one standard deviation, CB-NGA cannot account for the NW directivity trend visible in the rock sites, nor does it fully account for 3D effects at some of the deep basin sites. Our simulation generally under-predicts PGV at shallow basin sites, possibly due to the limited bandwidth of our model.

[K] Plot of PGV values from panel [J]. Error bars indicate one standard deviation to either side of the Campbell and Bozorgnia expected PGV.

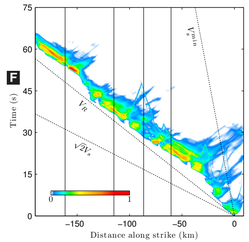

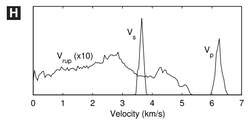

J

Table 1: Peak ground velocity (geometric mean horizontal component) compared to the Campbell and Bozorgnia (2007) NGA ground motion relation.

	R_{RUP}	$Z_{2.5}$	V_{S30}	PGV (cm/s)		
Rock sites	(km)	(km)	(m/s)	CB	SORD	POE
Yuma	123.0	0.0	2887	3.9	1.2	99%
Ensenada	184.2	0.0	3065	2.9	1.5	89%
San Diego	144.6	0.0	3028	3.5	2.6	71%
Oceanside	102.9	0.0	2787	4.4	4.0	58%
Victorville	33.3	0.0	3030	10.0	9.5	54%
Barstow	80.4	0.0	3245	5.3	6.3	37%
Lancaster	74.0	0.0	2555	5.6	7.0	34%
Bakersfield	183.7	0.0	2945	2.9	4.7	18%
Santa Barbara	202.8	0.0	2712	2.7	5.3	10%
Shallow basin sites						
Palm Springs	11.7	0.2	844	25.0	14.0	87%
San Bernardino	6.9	0.5	503	48.0	32.3	78%
Riverside	26.5	0.4	914	13.7	9.7	75%
Ontario	28.7	0.5	759	14.6	14.2	52%
Deep basin sites						
Mexicali	80.4	2.7	874	6.7	7.0	47%
Coachella	3.8	2.8	844	47.7	63.1	30%
Montebello	64.0	3.4	603	10.7	22.3	8%
Santa Ana	69.2	2.4	584	9.6	14.2	23%
Long Beach	86.0	2.8	524	8.7	12.9	23%
Los Angeles	73.5	2.7	606	9.0	9.1	49%
Westwood	88.2	3.1	717	7.3	7.4	49%
Oxnard	154.9	3.0	539	5.6	11.2	9%

Notes:
R_{RUP} is the closest distance to the coseismic rupture surface.
$Z_{2.5}$ is the depth to the 2.5 km/s shear velocity horizon.
V_{S30} is the average shear velocity for the upper 30 m.
CB PGV is the expected value from the ground motion relation.
SORD PGV is the simulated value.
POE is the probability of exceedance.